Evaluation and Improvement of an Inflow-Nudging Technique for Idealized Simulations of Convective Boundary Layers

CHRISTIAN H. BOYER[a] AND JASON M. KEELER[a]

[a] Department of Earth and Atmospheric Sciences, Central Michigan University, Mount Pleasant, Michigan

(Manuscript received 3 February 2022, in final form 15 September 2022)

ABSTRACT: Recent idealized modeling studies have highlighted the importance of explicitly simulating realistic convective boundary layer (CBL) structures to assess and represent their influence on mesoscale phenomena. The choice of lateral boundary conditions (LBCs) has a substantial impact on these turbulent structures, including the distribution of kinematic and thermodynamic properties within the CBL. While use of periodic LBCs is ideal, open LBCs are required for nonuniform domains (e.g., multiple air masses or land surface types). However, open LBCs result in an unrealistic, laminar CBL structure near the upstream boundary that undoubtedly impacts the evolution of any simulated phenomena. Therefore, there is a need for a modified open LBC option to mitigate this unrealistic structure, while still permitting users to simulate phenomena in nonuniform domains. The Pennsylvania State University–NCAR Cloud Model 1 (CM1), version 19.8, includes an optional inflow-nudging technique to nudge inflow to the base-state wind profile. For the present study, the authors modified this method to one that nudges toward a continually updated, horizontally averaged profile so that the technique may be used for phenomena under evolving conditions. Simulations using LBC choices, including nudging to either the base state or horizontal average, were evaluated relative to respective dual-periodic LBC control simulations with or without vertical wind shear. The horizontal average nudging technique outperformed the traditional open LBCs and nudging to the base state, as demonstrated using a histogram matching technique applied to grid points within the CBL. Ultimately, this work can be used to assist modelers in assessing which LBCs are appropriate for their intended use.

KEYWORDS: Convection; Boundary layer; Boundary conditions; Idealized models; Mesoscale models; Model evaluation/performance

1. Introduction

Over the last several decades, results from numerous field campaigns have established the critical influence of convective boundary layer (CBL) heterogeneities, such as open/closed cell convection and horizontal convective rolls, on the dynamics of mesoscale phenomena, including supercells (Bluestein et al. 2014; Lyza and Knupp 2018; Markowski et al. 2019), convection initiation (Friedrich et al. 2008a,b), and sea breezes (Atkins et al. 1995; Kingsmill 1995). As it has become computationally feasible, there has been a gradual shift in the mesoscale modeling community to include CBL heterogeneity in large-eddy simulations (LES), thus resulting, in theory, in simulations with turbulent characteristics and convective evolution that more realistically represents the atmosphere. Notable contributions to simulating realistic CBL have been made for a range of phenomena, including supercells (Nowotarski et al. 2014, 2015), sea/lake breezes (Dailey and Fovell 1999; Fovell and Dailey 2001; Fovell 2005) and drylines (Peckham et al. 2004; Xue and Martin 2006a,b). Nowotarski et al. (2015) evaluated the influence of boundary layer horizontal convective rolls and their associated horizontal heterogeneities on the evolution of supercells, while Dailey and Fovell (1999) found that the intersection of horizontal convective rolls and the seabreeze front produced stronger updrafts and a deeper front than simulations without horizontal heterogeneities. LES with realistic CBLs have become increasingly more common in recent years and will continue to be used more frequently in the future to further understand the effects that CBL heterogeneity has on various mesoscale processes. In addition to simulating a more realistic CBL, other recent advances have enabled representation of spatially varying atmospheric profiles using the base-state substitution method (Davenport et al. 2019) and maintenance of vertical wind profiles in simulations with surface friction (Dawson et al. 2019). However, Davies-Jones (2021) noted the potential for excessive shear near the surface when using the method introduced in Dawson et al. (2019).

Because of their relative simplicity and lower computational expense, idealized simulations that neglect friction, radiation, and surface fluxes are still common and useful in understanding certain aspects of mesoscale phenomena. In such environments, the homogeneous boundary layer and lack of diurnal variation enables use of open boundary conditions where features (e.g., cold pools) can exit the domain, while kinematics at the upstream lateral boundary are prescribed by the normal component of velocity, given by the radiative wave tendency equation (Mayor et al. 2002). Values for thermodynamic variables are prescribed assuming gradients normal to the lateral boundary are zero.

In simulations with model settings that produce a heterogeneous CBL [i.e., semislip surface, radiative parameterization, surface fluxes, and perturbations to the base state at initialization (Nowotarski et al. 2014)], use of open lateral boundary conditions (LBCs) results in an unrealistic laminar inflow region characterized by little variability in the along-flow direction, and large variability in the cross-flow direction for all kinematic and thermodynamic variables. This appearance is

Corresponding author: Jason M. Keeler, keele1j@cmich.edu

DOI: 10.1175/JAMC-D-22-0017.1

an artifact of the manner in which inflow characteristics are prescribed by the radiative wave tendency equation (Mayor et al. 2002) and may give the false impression of a convective roll-like structure, when in fact the flow is laminar. These structures may contribute to a destructive trend of the net mass inflow or outflow (Mayor et al. 2002) and may extend up to one hundred or more grid points within the domain at the upstream boundary before the simulation spins up.[1] The flow downstream is highly dependent upon the conditions that are prescribed at the upstream boundary and tend to overcompensate this transition between the eddy-deficient laminar inflow to the turbulent eddies within the center of the domain in simulations that only apply open LBCs (Lund et al. 1998; Gaudet et al. 2012). While periodic LBCs may be used to eliminate these unrealistic structures, this is only feasible in cases where the domain consists of a single air mass and uniform surface characteristics. Otherwise, any airmass boundary that exits the domain will reenter at the opposite lateral boundary. In addition, in cases of simulated deep moist convection, even if an outflow boundary does not exit the domain, the anvil may exit the domain and reenter such that the storm will shade its own inflow region. As a result, use of periodic LBCs requires a sufficiently large domain to prevent key features from exiting and reentering the domain, a solution that is often prohibitively computationally expensive. Therefore, there is a need for a solution that enables use of open LBCs, while minimizing the extent and downstream effects of laminar inflow. Previous efforts to alleviate the impact of open LBCs have done so through modification of the inflow. We categorize these inflow modification methods into the following: 1) asynchronous techniques that rely on calculations made outside of the model integration (e.g., Lund et al. 1998; Mayor et al. 2002; Gaudet et al. 2012; Bryan et al. 2017) and 2) synchro-nous techniques that occur during model integration (e.g., Skyllingstad et al. 2007; Mirocha et al. 2014; Muñoz-Esparza et al. 2014).

An asynchronous method developed by Lund et al. (1998) relies on model output from a periodic LBC simulation that is run separately. The authors extracted velocity characteristics from a plane within the asynchronous (precursor) periodic LBC simulation near the downstream lateral boundary. These velocity characteristics were then rescaled and recycled at the inflow boundary of the main open LBC simulation using a method based on earlier work by Spalart and Leonard (1985), resulting in more realistic turbulent inflow characteristics. Gaudet et al. (2012) developed a similar method that generates eddies in a separate periodic LBC simulation and injects them into the mesoscale flow, resulting in a decreased horizontal extent of the laminar inflow region. A slightly different approach that still relies on a precursor simulation is introduced in Mayor et al. (2002). For this method, the mean inflow profile is calculated using output from a precursor simulation and is held constant throughout the entire main simulation. Perturbations are added to the mean profile at the upstream lateral boundary, based on calculated perturbations from the main simulation at a vertical plane several kilometers downstream, referred to as the "magic slice." Asynchronous methods have also been used for the Pennsylvania State University–NCAR Cloud Model 1 (CM1; Bryan and Fritsch 2002) to inject eddies from a precursor periodic simulation into the main simulation (Bryan et al. 2017). While these asynchronous techniques are viable approaches, the frequent need to read data during the simulation results in computationally expensive experiments (Sever et al. 2019), compounding the added computational expense of requiring a periodic LBC simulation to be run beforehand. Moreover, if the user were to extend this work to use in simulations with multiple air masses in the domain, an additional simulation would be required to generate eddy properties and/or mean profiles for each air mass. For these reasons, the authors explored the use of synchronous methods.

Synchronous techniques are beneficial, in that they do not require a separate precursor simulation. One such example is that of Skyllingstad et al. (2007), which uses recirculated flow through a plane within the domain to set the upstream LBC, with adjustments made to ensure mass continuity. A synchronous technique developed by Mirocha et al. (2014) makes use of a domain consisting of two inner nests within a dual-periodic LBC outer domain. Random potential temperature and horizontal velocity perturbations are applied within the inflow region of the first nest. The combination of nesting and perturbations enabled turbulent eddies to spin up faster than simulations without the perturbed inflow, relative to a dual-periodic control simulation whose size and grid spacing were consistent with the inner nest. Similar methods were developed and evaluated by Muñoz-Esparza et al. (2014), who also found improvement in simulated structure relative to a dual-periodic LBC control simulation. While these methods are applicable to single airmass domains, their reliance on an outer domain with periodic LBCs precludes use of these methods for simulations with multiple air masses or nonuniform surface characteristics.

The limitations of the aforementioned asynchronous and synchronous techniques have motivated evaluation of an alternate technique that uses open LBCs and nudges inflow to a given profile, as in Mayor et al. (2002). In this paper, test simulations were employed with and without the use of inflow-nudging on open LBCs using CM1 (Bryan and Fritsch 2002), release 19.8, in environments with and without vertical wind shear. The inflow-nudging techniques used in the test simulations included nudging to either the base state or domainwide horizontal average wind profiles. In contrast to the method of Mayor et al. (2002), the method used herein introduces domainwide perturbations to the base-state profile only at model initialization to enable development of turbulence. The turbulent characteristics, kinematics, and thermodynamics within the CBL of the test simulations were evaluated against the respective shear or no-shear dual-periodic LBC simulation. The domainwide horizontal average inflow-nudging technique, introduced in this paper, was designed for further adaptation to nonuniform domains to simulate mesoscale phenomenon with a realistic CBL. While this method is intended

[1] Model spinup refers to both the time and space required to generate turbulence.

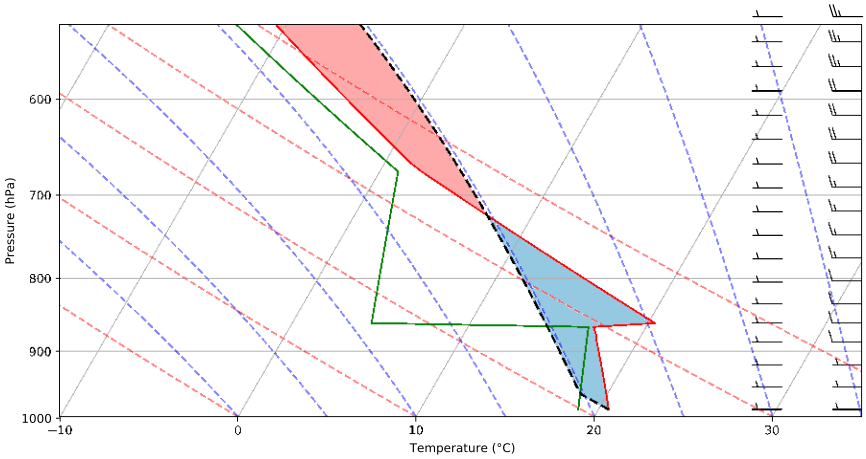

FIG. 1. Base-state sounding, including wind barbs (m s^{21}) for the no-shear (left barbs) and shear (right barbs) simulations. The dashed line is for the surface parcel path, and CIN (blue shading) and CAPE (red shading)are indicated.

for adaptation to use in nonuniform domains, a single airmass domain with uniform surface characteristics was necessary for this assessment so that a dual-periodic LBC control simulation with no laminar inflow was feasible. The remainder of the paper will be structured as follows. In section 2 we describe the methods and configuration of the simulations and associated analyses, while section 3 presents the results. A discussion is given in section 4, followed by conclusions and a summary in section 5.

2. Methods

Two sets of seven simulations were performed, each using a different LBC, to evaluate the impact of LBC choice on the nature of the simulated CBL, under conditions with and without vertical wind shear. All simulations were run using CM1, release 19.8 (Bryan and Fritsch 2002). Aside from LBC differences and whether vertical wind shear was present, the model configuration and initial conditions were constant across all simulations.

a. Model configuration and base state

For all simulations, the model domain was 904 3 100 3 56 grid points in the west–east, south–north, and vertical dimensions with a horizontal gridpoint spacing of 100 m and a vertical-level spacing of 50 m in the lowest 2 km AGL. The vertical-level spacing was gradually increased from 50 m at 2 km AGL to 250 m at and above 3.5 km AGL. This resulted in a domain size of 90.4 km 3 10 km 3 5 km in the west–east, south–north, and vertical dimensions. The simulation was run for 180 min (3 h) starting at 1500 UTC with a large model time step of 1 s, and output generated every 5 min. The 3-h length of the simulation was sufficient for the development and evolu-tion of turbulent eddies within the boundary layer and, in future applications, would be sufficient to study the evolution of mesoscale phenomena. The NASA Goddard radiation scheme was used, with radiative tendencies updated every 180 s for a reference latitude of 408 and a longitude of 21008 for 15 July. The bottom boundary condition was semislip to allow for frictional effects and a free slip upper boundary condition with a Rayleigh damping zone above 2.5 km AGL was used. The base-state wind profile for the no-shear simulations set u 5 5 m s^{21} and y 5 0 m s^{21} for the full depth of the domain (Fig. 1 left barbs) while the shear simulations set u 5 5 m s^{21} at the lowest model level and increased u by 4 m s^{21} km^{21} through the domain top (Fig. 1, right barbs). As was the case in the no-shear simulations, y was constant at 0 m s^{21}. The base-state thermodynamic pro-file was characterized by a capping inversion at approximately 875 hPa with a weakly stable layer below and a well-mixed layer above (Fig. 1). At initialization, random potential temperature perturbations with magnitudes up to 0.1 K were added to the base-state value at all grid points in the lowest 10 vertical levels to introduce sufficient boundary layer heterogeneity to enable development of a realistic CBL. Full details of the model configuration are provided in Table 1.

These two experiments were configured to evaluate a set of simulations in a pseudo-2D model domain with uniform surface characteristics, relative to a control (CON) simulation with dual-periodic LBCs in both no-shear and shear environments. The other six boundary condition simulations are as follows: Open (OPEN), open with nudging to the base state (BS), open with nudging to the horizontal average (AVG), open west–east with periodic north–south boundary conditions (OPEN PNS), open west–east with nudging to the base state and periodic north–south boundary conditions (BS PNS), and open west–east with nudging to the horizontal average and periodic north–south boundary conditions (AVG PNS). The periodic, open, and open with nudging to the base-state LBC options are standard and available within CM1. The open with nudging to the horizontal average technique was developed by the authors and implemented within CM1 based on the base-state nudging method. Typically, open boundary conditions prescribe the value of the first grid point within the domain at the upstream boundary. When the base-state nudging is added to open LBCs, the value prescribed at

TABLE 1. Model configuration.

Parameter	Description
Model	CM1, release 19.8
Grid points	904 3 100 3 56 grid points
Horizontal grid spacing	100 m
Vertical-level spacing	50 m below 2 km AGL; gradually increase to 250 m at 3.5 km AGL and above
Domain extent	90.4 km 3 10 km 3 5 km
Radiation scheme	NASA Goddard
Reference location	408; 21008
Advection scheme	Fifth-order advection
Pressure solver	Klemp–Wilhelmson time-splitting; vertically implicit
Subgrid-scale parameterization	TKE scheme
Lateral boundary conditions	Varies
Bottom boundary condition	Semislip
Top boundary condition	Free slip with Rayleigh damping zone above 2.5 km AGL
Random temperature perturbations	0.1 K
Land surface type	Irrigated cropland and pasture
Surface roughness	$10 3 10^{22}$ m
Nudging time scale (when applicable)	20 s

the upstream boundary is instead nudged toward the base state. In the case of open LBCs with nudging toward the horizontal average, the upstream boundary was nudged toward the domainwide horizontal average at each vertical level. Inflow nudging is only applied to u on west or east lateral boundaries, and y on south or north lateral boundaries. In situations where there are two velocity components in the inflow, nudging is applied at any boundary with inflow. For example, in the case of a simulation with southwest flow, inflow at the western boundary would be nudged to the u component of the wind while inflow at the southern boundary would be nudged to the y component of the wind. The nudging tendency is calculated by

$$u_{ten} 5 u_{ten} 2 (u 2 u_0)\frac{1}{a} \quad \text{and} \tag{1}$$

$$y_{ten} 5 y_{ten} 2 (y 2 y_0)\frac{1}{a}, \tag{2}$$

where u_{ten} and y_{ten} are the calculated velocity tendency due to nudging at every grid point at the inflow boundary, u and y are the velocity at every grid point at the inflow boundary, u_0 and y_0 are either the base state at every grid point at the inflow boundary or the calculated domainwide horizontal average velocity at each vertical level, and a is the time scale of the nudging tendency.

For test simulations where nudging the inflow to the base state or domainwide horizontal average was employed, the nudging time scale was 20 s. Since all simulations were identical aside from LBCs (within the no-shear or shear sets of simulations), the extent to which statistical properties of CBL characteristics in the other no-shear/shear simulations match their respective control simulation can be interpreted as an evaluation of their relative performance. In future work, the newly developed nudging to the horizontal average option will be adapted for use in inhomogeneous domains (e.g., multiple surface types or multiple air masses) so that the horizontal average calculated for inflow nudging is occurring within a representative portion of the inflow boundary's respective air mass.

b. Analysis

The open LBC simulations were evaluated in comparison with the dual-periodic control simulation, qualitatively and quantitatively, using kinematic (u, y, w) and thermodynamic variables (u, q_y). Additionally, the average turbulent kinetic energy (TKE) was calculated at each vertical level to compare the turbulent characteristics between simulations. A histogram matching score (hh), introduced in Swain and Ballard (1991), was used to quantitatively compare the intersection of histograms of individual thermodynamic and kinematic variables from the six open LBC simulations with those of the dual-periodic control simulation. Model output used to generate the histograms and their matching scores was limited to the to the lowest 975 m (first 20 model levels) to allow for all of the distributions of the seven simulations to be fully within the boundary layer at all times. This histogram matching score was calculated by

$$hh 5 \frac{\sum_{j51}^{n} \min(K_j, L_j)}{\sum_{j51}^{n} K_j}, \tag{3}$$

where K was the histogram of the dual-periodic control simulation, L was the histogram of one of the six remaining open LBC simulations, and n was the number of bins of the histogram. The histogram matching score was given by calculating the histogram intersection (numerator) of a histogram K of the dual-periodic control simulation, and the histogram L of the other simulated distributions (Swain and Ballard 1991; Koch et al. 2018). The histogram intersection was then normalized (denominator), resulting in a score between 0 and 1, with hh 5 1 indicating a perfect intersection of the two histograms and hh 5 0 indicating no overlap. The parameters used for the histograms and to calculate the histogram matching

TABLE 2. Parameters used for histogram matching score calculation.

Simulation set	Variable	Range	No. of bins	Bin width
No shear	u	294–303 K	180	0.05 K
	u	from 29 to 11 m s^{21}	200	0.1 m s^{21}
	y	from 29 to 11 m s^{21}	200	0.1 m s^{21}
	w	from 25 to 7 m s^{21}	120	0.1 m s^{21}
	q_y	0.011–0.017 g kg^{21}	200	3 3 10^{25} g kg^{21}
Shear	u	294–305 K	220	0.05 K
	u	from 28 to 13 m s^{21}	210	0.1 m s^{21}
	y	from 28 to 13 m s^{21}	210	0.1 m s^{21}
	w	from 26 to 9 m s^{21}	150	0.1 m s^{21}
	q_y	0.008–0.017 g kg^{21}	300	3 3 10^{25} g kg^{21}

score are provided in Table 2. The range of values for individual variables was set so that the minimum and maximum values across all output times in all simulations were included, resulting in consistency across all calculations of hh. In addition, the bin width was consistent across individual kinematic variables. The calculated hh values and distributions were also inspected using time series and distance series.

3. Results

a. CON without shear

CON was run using periodic boundary conditions applied to all lateral boundaries to simulate a realistic CBL. Weak turbulent eddies were discernible across the entire domain by 10 min into the simulation, as seen in the lowest model level's w field (Fig. 2a). As the simulation progressed, these eddies became stronger, with a more coherent structure at 40 min that evolved into a hexagonal-shaped pattern by 80 min, indicating the development of shallow mesoscale cellular convection within the boundary layer (Figs. 2b,c). Cellular convection is the favored convective mode over roll convection when the vertical wind shear is less than 10^{23} s^{21} (Miura 1986). This was consistent with the base-state vertical wind profile, as there was initially zero vertical wind shear present through the entire depth of the domain (Fig. 1). More specifically, the cells that developed within the control simulation were open-cell convection, as the interior of the cells had weak descending motion, surrounded by a relatively narrow ring of stronger ascending motion (Fig. 2), as in Helfand and Kalnay (1983). A contoured-frequency-by-time diagram (CFTD) is shown to visualize this process. CFTDs are generated by isolating model output from a subset of the domain (i.e., up to 975 m AGL) and sorting grid points within that domain subset into bins based on their values for a given parameter. Histograms of the fraction of grid points in each bin and how they change in time are summarized in one figure (Keeler et al. 2016), where the sum of fractions for all bins at a given time is equal to 1. Herein, a CFTD of w illustrates the development of convection in the CBL. For the control simulation, the CFTD shows that there was a higher frequency of grid points within weak downdrafts and a lower frequency of grid points within stronger updrafts. These stronger individual updrafts resulted in a larger maximum magnitude of w for updrafts than downdrafts, as the 99th-percentile contour approached 3 m s^{21} while the 1st-percentile contour only

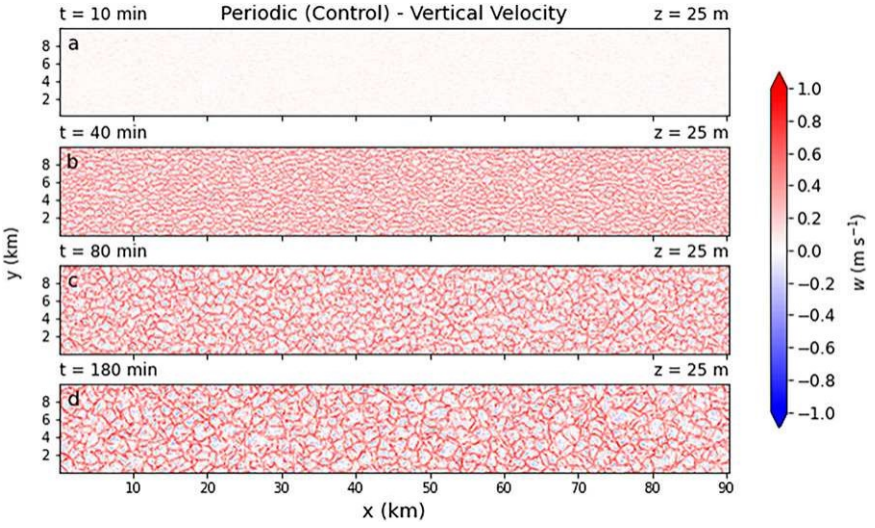

FIG. 2. 25-m (AGL) vertical air velocity for the no-shear control simulation at (a) 10, (b) 40, (c) 80, and (d) 180 min.

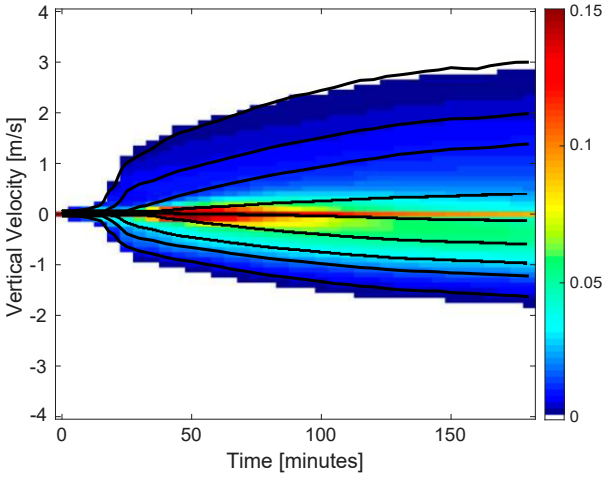

FIG. 3. Vertical air velocity CFTD of the no-shear control simulation in the lowest 975 m of the domain with the contours showing the 99th (top contour), 95th, 75th, 50th, 25th, 10th, 5th, and 1st (bottom contour) percentiles.

approached 22 m s^{21} (Fig. 3). In addition, open-cell convection occurs when the bottom layer of the atmosphere warms, forcing the air to rise, which in our simulation was due to the warming of the model surface by insolation (Helfand and Kalnay 1983). Therefore, as the simulation progressed and insolation increased, the warming of the surface allowed the air to become unstable and force the air to ascend resulting in the generation of the open-cell convection. The size of the individual convective cells was noticeably larger by 80 min (Fig. 2c); however, by the end of the simulation at 180 min, the CBL depth extended from the surface to the base of the capping inversion and the eddies seemingly reached a pseudo–steady state in terms of size and pattern. Further deepening (and widening) of cells was likely limited by the strong capping inversion (Fig. 1). The w distribution continued to gradually broaden through the end of the simulations, which was approximately 46 min prior to solar noon (Figs. 2d, 3).

b. OPEN without shear

As discussed in section 3a, CON generated turbulence and open-cell convection across the entire domain as seen in 25 m AGL plan views of u, u, and y at 180 min (Figs. 4a, 5a, 6a). However, in stark contrast to CON, the simulations that applied open LBCs include a region of laminar inflow at the western (upstream) lateral boundary that gradually transitions into turbulent, open-cell convective structures. The distance required for this transition varies between simulations, as seen in u, u, and y at 180 min (Figs. 4b–g, 5b–g, 6b–g). While readers may infer differences between the simulations by visually inspecting these plan views, quantitative differences between the simulations will be discussed in the following sections focused on overall characteristics of the full domain at

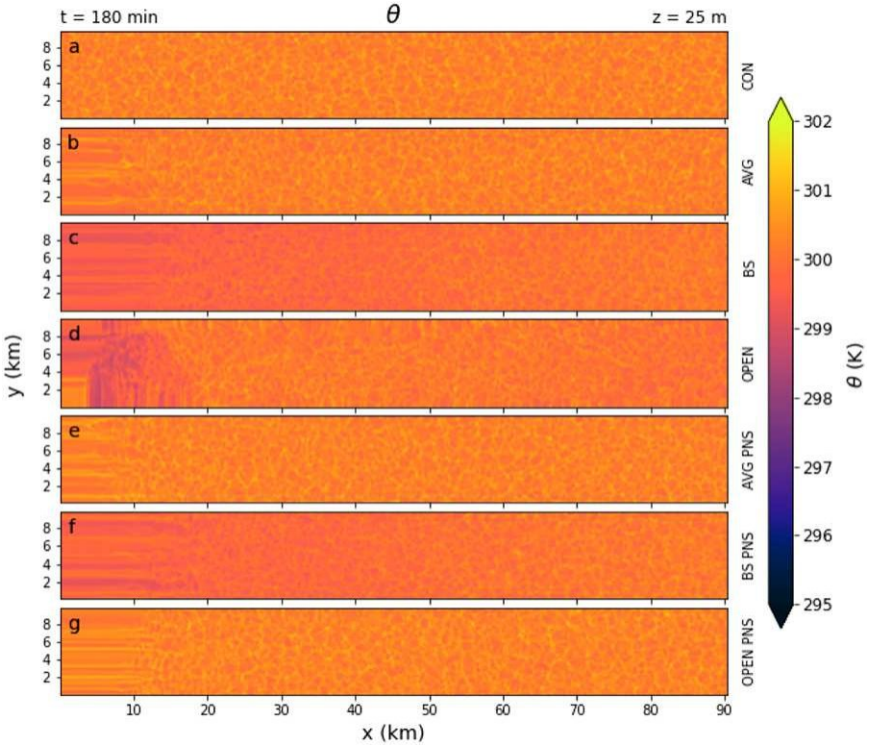

FIG. 4. Plan view of u at 180 min at the lowest model level (25 m) for no-shear simulations including (a) CON, (b) AVG, (c) BS, (d) OPEN, (e) AVG PNS, (f) BS PNS, and (g) OPEN PNS. See the text for the definitions of the simulation names.

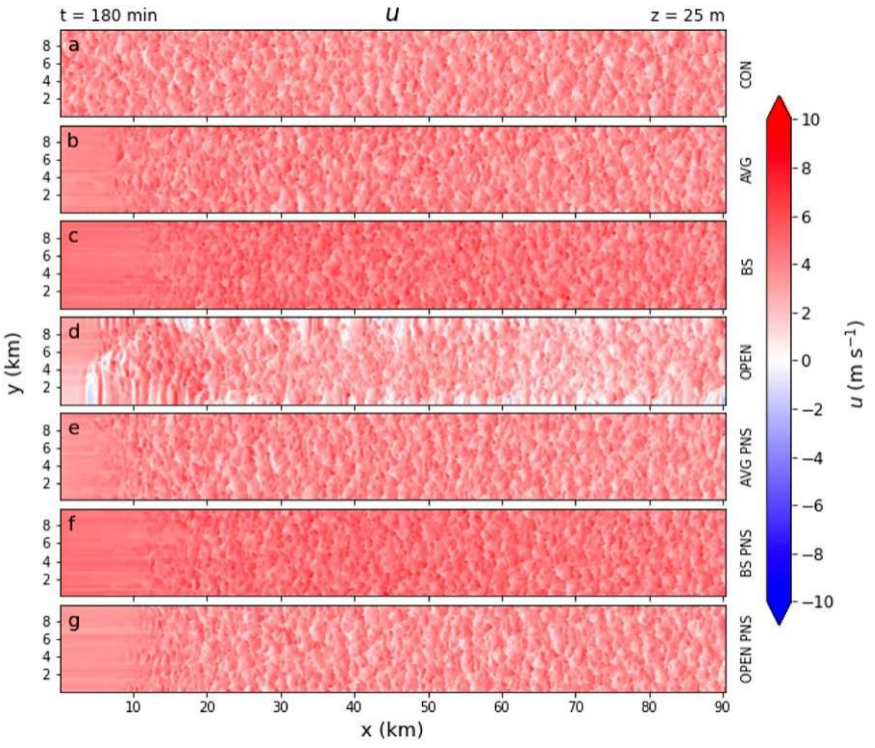

FIG. 5. As in Fig. 4, but for u.

180 min, spatial differences at 180 min, and how differences between simulations evolved from 0 to 180 min.

1) FULL DOMAIN CHARACTERISTICS AT 180 MIN

At 180 min in OPEN (west–east and north–south), the overall domain tended to be cooler than CON (Fig. 4d), especially in the western 20 km of the domain. Overall, the 50th percentile of the u was 0.176 K cooler than CON within the boundary layer. This appeared to be related to the area of laminar inflow in the western ;20 km of the domain (Fig. 4d). These differences resulted in a relatively low histogram matching score of 0.6081 (Fig. 7c). Key differences between OPEN and CON can also be seen in the u and y distributions (Figs. 5d, 6d). At 180 min, the 50th percentile of u was 0.756 m s^{21} lower, and y had a wider range of values (from 28.278 to 7.140 m s^{21}) for OPEN and (from 23.883 to 4.103 m s^{21}) for CON (Figs. 8c, 9c). These differences in the kinematic fields resulted in histogram matching scores of 0.6378 and 0.8099 for u and y, respectively. In addition to the substantial statistical differences for these variables, plan views for OPEN consist of zonally oriented stripes of higher and lower values that are intercepted by what appears to be a meridionally oriented pattern of constructive and destructive interference. These structures seen in OPEN are in stark contrast to CON and are not supported dynamically by the base-state environment. Moreover, the domain-average profile of TKE for OPEN is a clear outlier when compared with all other simulations with a RMSE 5 0.8616 m^2 s^{22} relative to CON in the lowest 975 m AGL, the largest error for any of the simulations (Fig. 10).

The open (west–east and north–south) LBC simulation with nudging to the BS more closely matched the domain-average TKE profile of CON in comparison with OPEN, with a RMSE 5 0.1118 m^2 s^{22} relative to CON in the lowest 975 m AGL (Fig. 10). However, other deficiencies arose when using this method. There was a positive bias in u relative to CON (Figs. 5c, 8b), with an increase in the 50th percentile of u of 1.072 m s^{21} through 975 m AGL, and a poor hh of 0.4167. This difference can be attributed to surface drag decreasing u relative to the base-state profile in CON. Despite the poor BS matching score for u, the BS matching score for y was nearly perfect (hh 5 0.9827) and was the highest for all simulations (Figs. 6c, 9b). Using the base-state nudging resulted in a substantial difference in the u field (Fig. 4c). The aforementioned positive bias in u near the upstream boundary resulted in convergence and weak ascent, thereby resulting in a cool bias. This cool bias decreased with eastward distance due to airmass modification through surface heat fluxes and subsequent vertical mixing. For example, the 50th percentile of u was 0.458 K lower in the western half of the domain and 0.182 K lower in the eastern half of the domain. These differences are also evident in the histogram matching score of 0.4565, which was the lowest score for u for any of the simulations (Fig. 7b).

The open (west–east and north–south) LBC with nudging to the AVG technique introduced herein improved many of the issues from OPEN and BS. Despite the laminar inflow continuing to be present, the inward extent was reduced to ;10 km (Figs. 4b, 5b, 6b). Additionally, the TKE spectrum

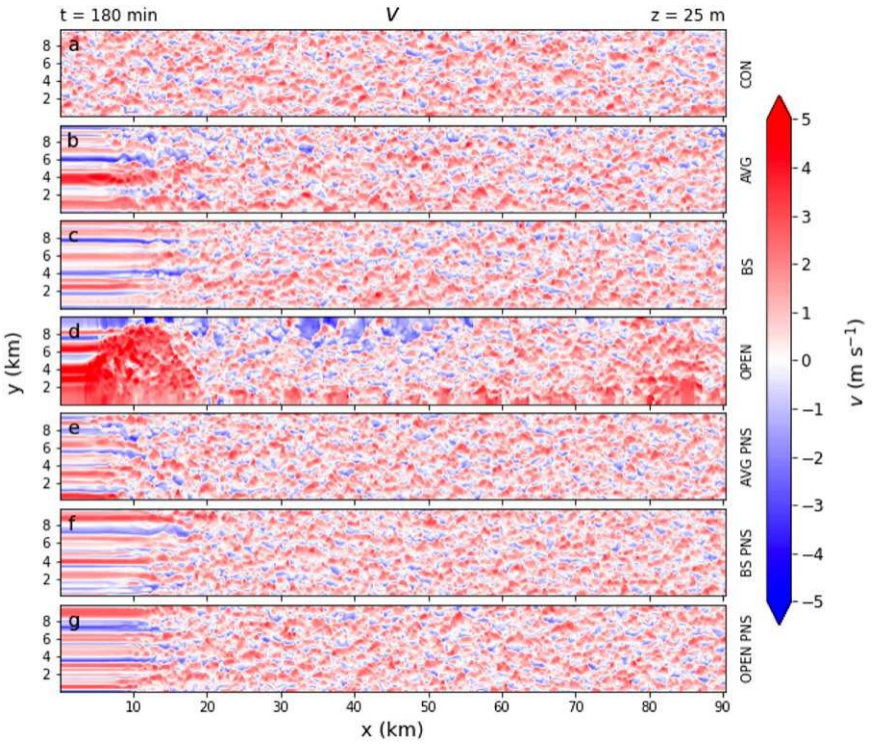

FIG. 6. As in Fig. 4, but for y.

was more comparable to CON than any of the other simulations that did not utilize periodic north–south LBC (see section 3c), with a TKE RMSE 5 0.1061 $m^2 s^{22}$ relative to CON in the lowest 975 m AGL (Fig. 10). The u distribution of AVG marked a substantial improvement relative to BS, with a minor difference in the 50th percentile of u of 0.027 K between AVG and CON and a high hh score of 0.9263 at 180 min (Fig. 7a). This represents the highest hh score for u among simulations without periodic north–south LBC. Similar improvements were seen with the distribution of u, as AVG performed better than both OPEN and BS. Despite a slight positive bias in the 50th percentile of u of 0.363 m s^{21} relative to CON, AVG had the highest hh (0.7863) of any simulation without periodic north–south LBC (Fig. 8a). The y distribution closely matched

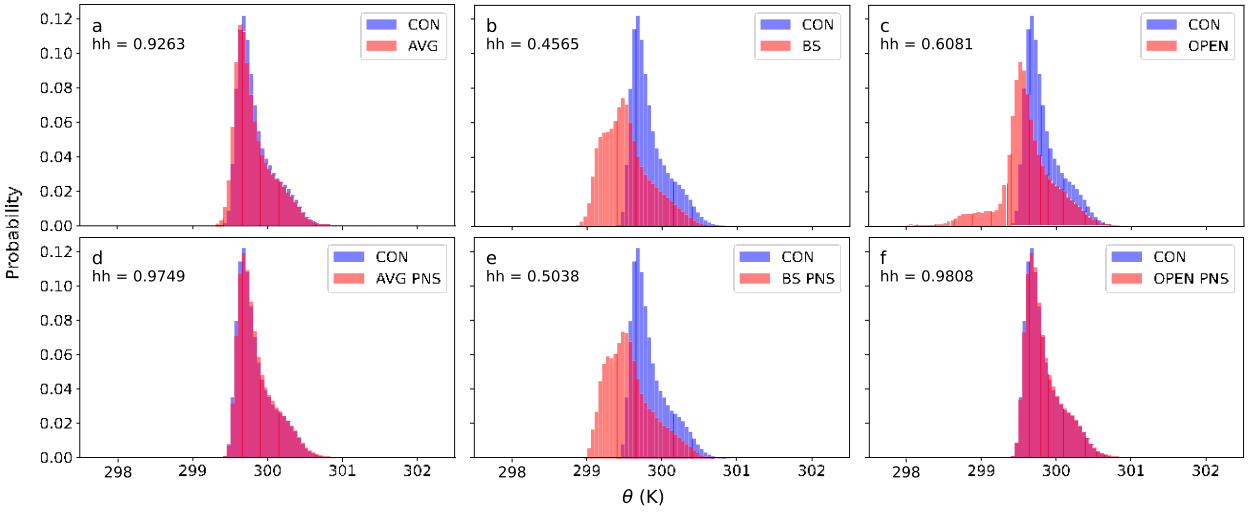

FIG. 7. Histograms and histogram matching scores for the no-shear simulations, comparing CON (blue) with (a) AVG, (b) BS, (c) OPEN, (d) AVG PNS, (e) BS PNS, and (f) OPEN PNS (red).

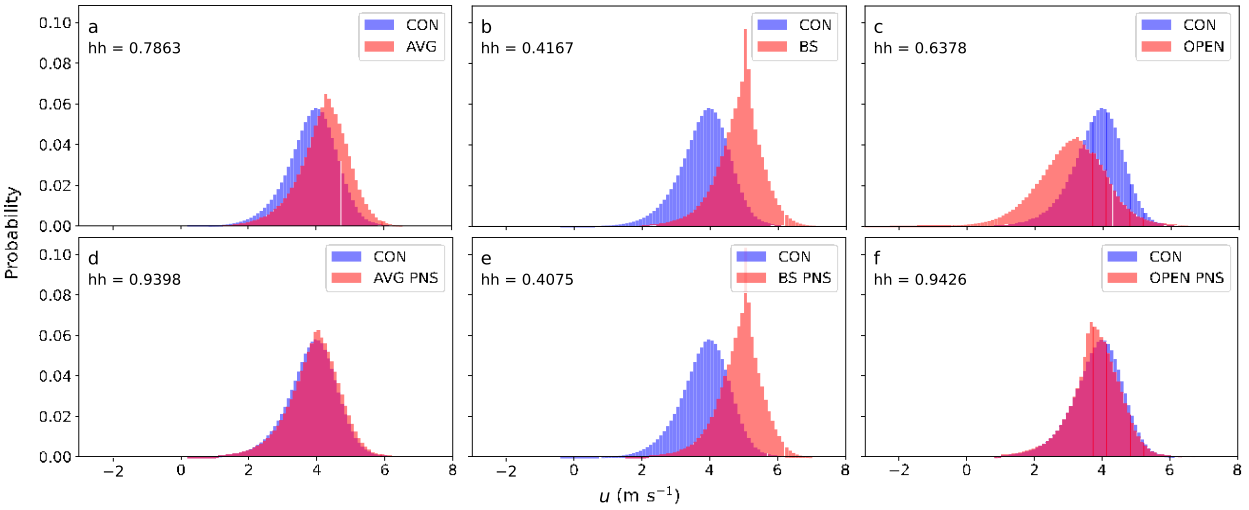

FIG. 8. As in Fig. 7, but for u.

that of CON (hh 5 0.9616) and was only 0.0211 lower than that of BS (hh 5 0.9827, Figs. 9a,b).

2) SPATIAL DIFFERENCES BETWEEN SIMULATIONS AT 180 MIN

To assess the performance of the test simulations relative to CON at varying locations in the domain, histogram matching scores were calculated in 10-km-wide subsets of the domain (Fig. 11) at 180 min. It was quite clear that the laminar inflow limited the performance of the model in the first 20 km downstream of the western lateral boundary. AVG performed the best among fully open LBCs across the entire domain while OPEN and BS perform poorly (Figs. 11a–c). For u, AVG's histogram matching score started at a higher value (hh 5 0.8182) than both OPEN (hh 5 0.2227) and BS (hh 5 0.2781) in the first 10 km and remained greater than the other two simulations across the domain (Fig. 11a). In addition, after having a histogram matching score of 0.6567 for u in the first 10 km, the score for AVG continues to increase throughout the remainder of the domain where the eastern 10 km of the domain has a score of 0.9141 (Fig. 11b). For y, the histogram matching increases from 0.7402 at the western boundary to greater than 0.98 by 30 km and remains near that value for the remainder of the domain (Fig. 11c). OPEN had a histogram matching score for u of 0.2227 and 0.4851 for 0–10 and 10–20 km, respectively, before improving to greater than 0.7 from 30 to 70 km (Fig. 11a). However, its performance began to fall off gradually toward the eastern boundary. In addition, u performs fairly well in the first 30 km (hh greater than 0.75) before decreasing across the rest of the domain and reaching a minimum of hh 5 0.3786 between 70 and 80 km. For y, OPEN consistently had a worse score across the entire domain than the other simulations. As for BS, the first half of the domain exhibits the low matching score due to the cool bias (Fig. 11a) and an

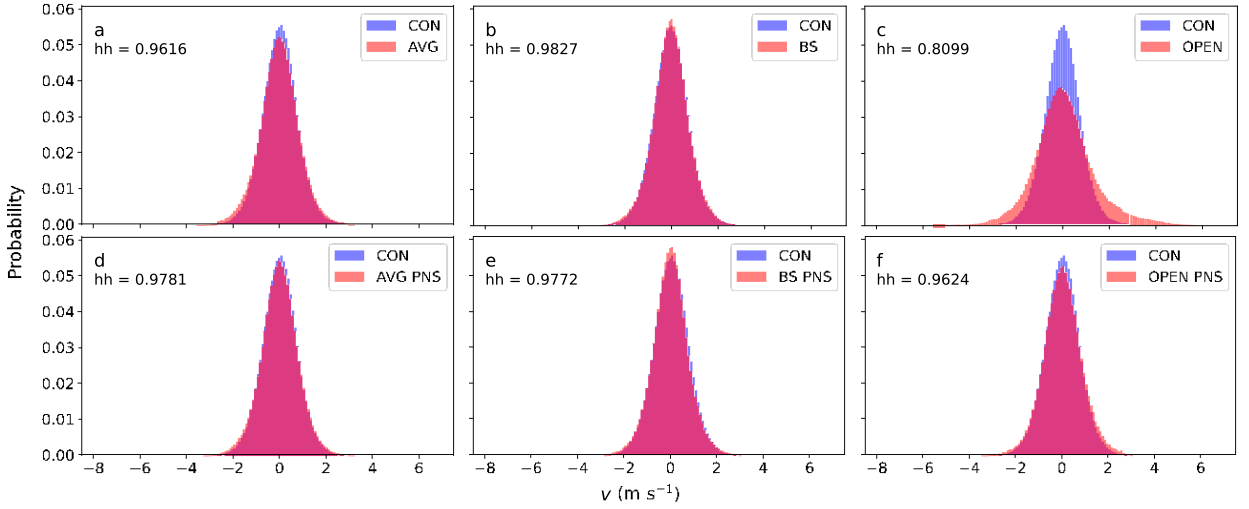

FIG. 9. As in Fig. 7, but for y.

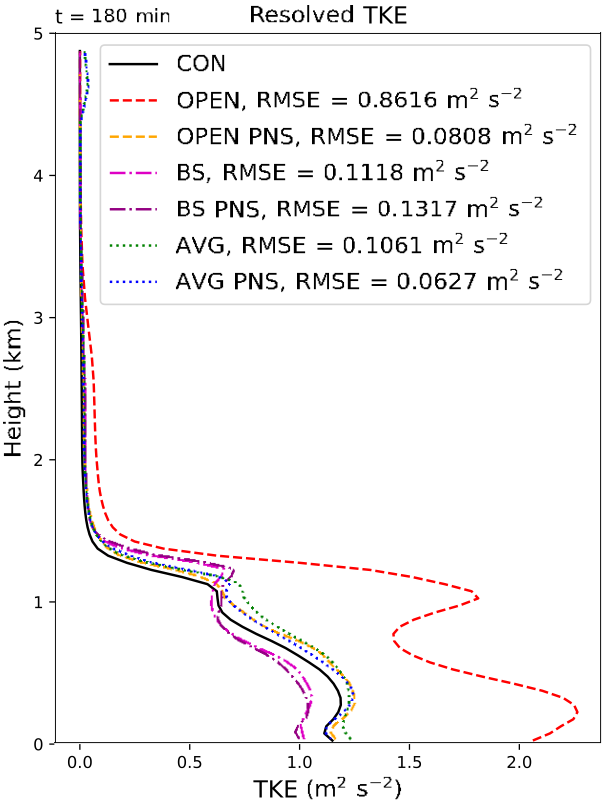

FIG. 10. Mean TKE profiles at t 5 180 min for the no-shear simulations. RMSE values relative to CON are calculated in the lowest 975 m.

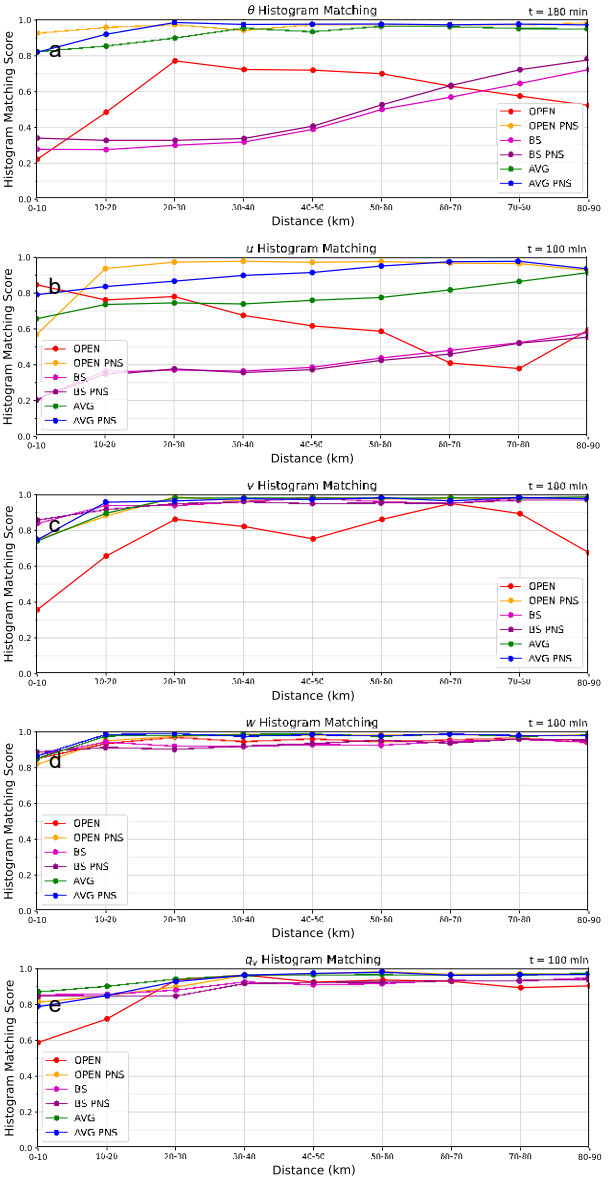

FIG. 11. Distance series of hh for the no-shear simulations at 180 min calculated for 10-km-wide subsets of the domain in the lowest 975 m for (a) u, (b) u, (c) y, (d) w, and (e) q_y.

overestimation in u (Fig. 11b), as discussed earlier, which causes its poor performance in the western 50 km of the domain, where the histogram matching score is less than 0.5 for both u and u. However, BS began to improve farther downstream, with the highest histogram matching scores occurring in the eastern 10 km (hh_u 5 0.7235, hh_u 5 0.5792). The y distance series started with a score of 0.8313 in the first 10 km, which was the highest among OPEN and AVG (Fig. 11c) and rose to greater than 0.93 by 10–20 km and remained above that value for the rest of the domain. The remaining variables of w and q_y did not have any major differences with the exception of OPEN having a poor histogram matching score of q_y in the western 20 km of the domain (Figs. 11d,e).

3) TEMPORAL EVOLUTION OF DIFFERENCES

Analysis of the performance of the histogram matching score with time revealed that the u and u distribution of AVG continued to perform the best throughout the length of the simulation among simulations without periodic north–south LBCs, with histogram matching scores consistently above 0.92 and 0.78, respectively. In marked contrast, hh for BS u declined rapidly to 0.6287 by 5 min and remained below 0.7 through the end of the simulation, when hh 5 0.4565 (Fig. 12b). Potential temperature did not have as immediate of a decrease in hh but exhibited a similar trend in the score decreasing with time (Fig. 12a). OPEN also exhibited poor performance when compared with AVG but consistently had a higher histogram matching score than BS for both u and u. The y histogram matching score is markedly higher than u and u, with the exception of OPEN (Fig. 12c), which began to decrease at 25 min and had the lowest histogram matching score at the final time step of 0.8099. The other simulations had relatively minor decreases in hh for y; however, hh remained at or above 0.9298 for the duration of the simulation. The lower hh for OPEN can be attributed to the larger magnitudes of y along both the north and south boundaries seen in Fig. 6d.

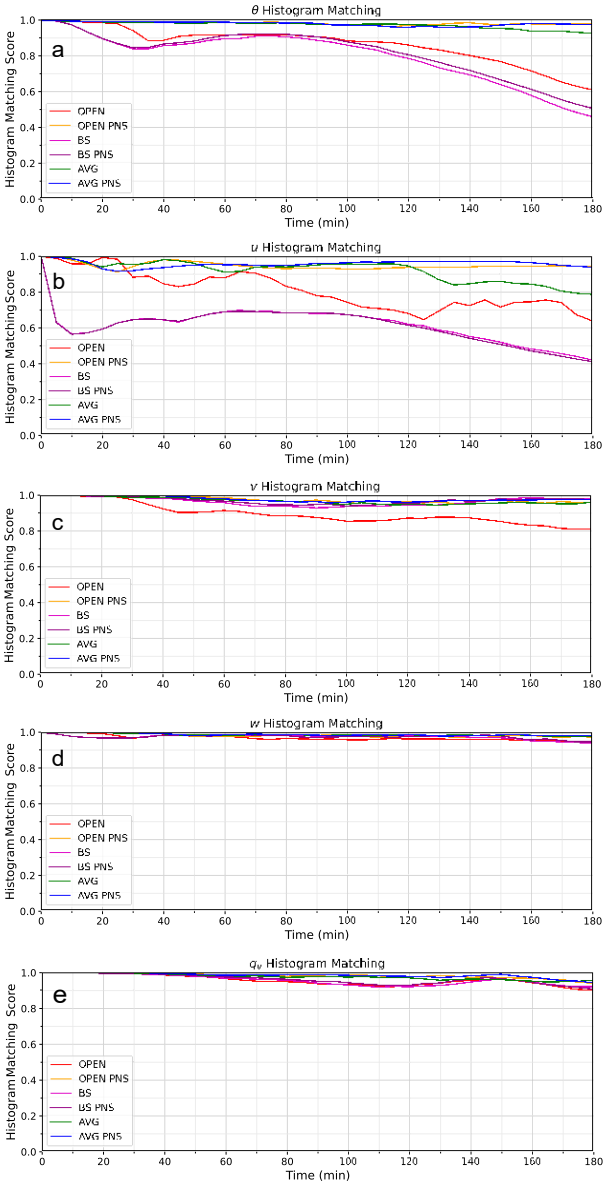

FIG. 12. Time series of hh for the no-shear simulations in the lowest 975 m of the full domain for (a) u, (b) u, (c) y, (d) w, and (e) q_y.

4) OPEN PNS

In addition to the simulations with no nudging (OPEN), BS, and AVG, a set of simulations was performed with periodic LBCs on the north–south boundaries, denoted PNS as mentioned above. Applying PNS LBCs decreased RMSE for TKE profiles and increased the histogram matching scores for AVG PNS and OPEN PNS relative to AVG and OPEN, respectively (Figs. 7d–f, 8d–f, 9d–f, 10). While OPEN PNS exhibited the largest improvement in TKE relative to its non-PNS counterpart (RMSE of 0.0808 vs 0.8616 $m^2 s^{22}$), AVG PNS had the lowest TKE RMSE of any simulations (0.0627 $m^2 s^{22}$). Interestingly, there was little difference between matching scores for BS PNS and BS, with BS PNS actually consisting of larger

TABLE 3. Histogram matching scores for the no-shear simulations at 180 min for grid points in the lowest 975 m of the domain. DIFF is the difference between the PNS simulations and the non-PNS simulations.

Simulation	u	u	y	w	q_y	Mean
OPEN	0.6081	0.6378	0.8095	0.9448	0.9011	0.780 26
BS	0.4558	0.4167	0.9831	0.9402	0.9199	0.743 14
AVG	0.9256	0.7863	0.9617	0.9782	0.9557	0.921 50
OPEN PNS	0.9810	0.9426	0.9624	0.9729	0.9435	0.960 48
BS PNS	0.5020	0.4075	0.9774	0.9463	0.9075	0.748 14
AVG PNS	0.9752	0.9398	0.9781	0.9820	0.9425	0.963 52
OPEN DIFF	0.3729	0.3048	0.1529	0.0281	0.0324	0.187 22 BS
DIFF	0.0462	20.0092	20.0057	0.0061	20.0124	0.005 00
AVG DIFF	0.0496	0.1535	0.0164	0.0038	20.0132	0.042 02

RMSE in TKE (Fig. 10; Table 3). While the simulation with the highest matching score was not consistent across all variables, differences in hh for individual variables were generally small between OPEN PNS and AVG PNS. To enable an overall comparison between all simulations, the mean hh across all variables is included in Table 3. In terms of histogram matching scores between PNS and non-PNS simulations, OPEN PNS exhibited the largest increase with a mean hh increase of 0.187 22. There was a small increase in the mean hh score of 0.042 02 for AVG PNS and a negligible increase in mean hh for BS PNS of 0.005 00. AVG PNS had the highest mean hh of 0.963 52, followed closely by OPEN PNS with a mean hh of 0.960 48. The mean hh score for BS PNS was substantially lower at 0.748 14. In summary, AVG PNS had the lowest TKE RMSE and highest mean hh score of any simulation.

5) HH WITH HEIGHT WITHIN THE BOUNDARY LAYER

Figure 13 includes hh for every vertical level at or below 975 m. In general, histogram matching scores for u were the highest in the upper CBL (Fig. 13a), as we see an increase in the mean hh for u (Fig. 13f). Furthermore, AVG, AVG PNS, and OPEN PNS continue to outperform the other three simulations throughout the depth of the CBL, as their hh scores never drop below 0.85 (Fig. 13a). For u, overall, the highest values of hh were closest to the surface (Figs. 13b,f.) In addition, AVG PNS and OPEN PNS do not exhibit any substantial differences from the lower model levels to the upper model levels of the CBL and have histogram matching scores greater than 0.92 at all levels. The histogram matching scores were generally consistent with height for both y and w, as most simulations had scores greater than 0.9, with y for OPEN being the only exception (Figs. 13c,d,f). For q_y, mean hh decreased with height above the 575 m model level (Fig. 13f), and was primarily driven by decreasing hh of BS, BS PNS, and OPEN, as those three simulations decrease more significantly than AVG, AVG PNS, and OPEN PNS.

c. Periodic and OPEN simulations with shear

The second set of simulations was identical to the first set, aside from including 4 m s^{21} km^{21} vertical wind shear for u

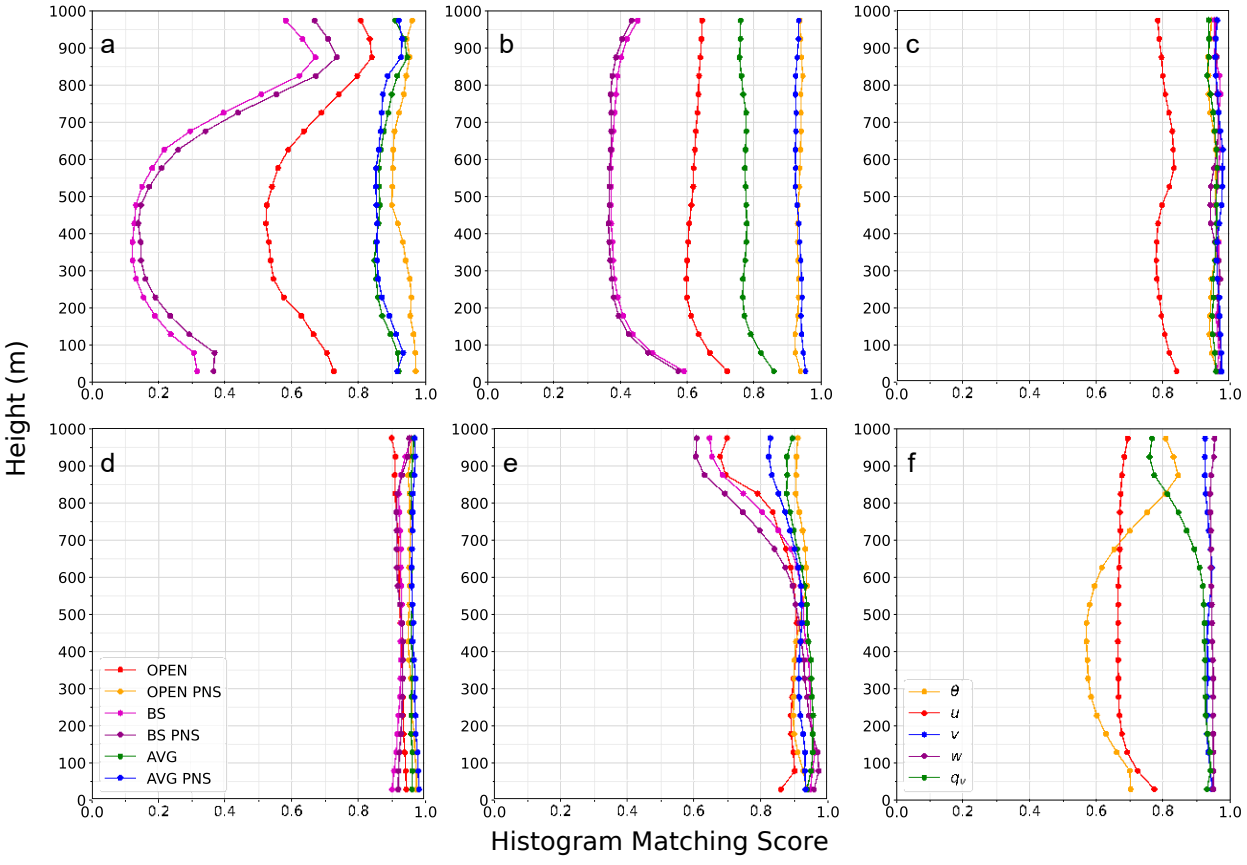

FIG. 13. Histogram matching scores (hh) for the no-shear simulations for (a) u, (b) u, (c) y, (d) w, (e) q_y, and (f) mean hh at every vertical level within the lowest 975 m of the domain.

and was completed to evaluate the nudging method in situations where the wind profile is not constant with height. As will be shown, results are generally consistent with the no-shear simulations, so a brief description of these simulations is provided.

As in the no-shear simulations, the mean hh score for the sheared simulations at t 5 180 min was highest for AVG (hh_{mean} 5 0.959 56), followed by OPEN (hh_{mean} 5 0.825 58), and BS (hh_{mean} 5 0.719 10, Table 4). When using periodic north–south LBCs, base-state nudging remained the lowest mean hh score, and the average and open scores were similar to one another (AVG PNS hh_{mean} 5 0.923 46, and OPEN PNS hh_{mean} 5 0.959 68). Unlike in the no-shear simulations, the AVG PNS hh_{mean} was slightly lower than the AVG hh_{mean}. This was due to a difference in matching score for u (AVG PNS hh 5 0.8175, as compared with AVG hh 5 0.9823). Despite this difference, AVG PNS still had the lowest TKE RMSE (Fig. 14).

In terms of spatial variation in hh at t 5 180 min, the base-state simulations with and without periodic north–south LBCs continue to have low histogram matching scores for u and u

TABLE 4. As in Table 3, but for the shear simulations.

Simulation	u	u	y	w	q_y	Mean
OPEN	0.7125	0.6707	0.8700	0.9609	0.9138	0.825 58
BS	0.4051	0.4250	0.9734	0.9315	0.8605	0.719 10
AVG	0.9120	0.9823	0.9865	0.9851	0.9319	0.959 56
OPEN PNS	0.9594	0.9498	0.9694	0.9734	0.9464	0.959 68
BS PNS	0.4408	0.4075	0.9776	0.9436	0.8553	0.724 96
AVG PNS	0.9120	0.8175	0.9795	0.9874	0.9209	0.923 46
OPEN DIFF	0.2469	0.2791	0.0949	0.0125	0.0326	0.134 10
BS DIFF	0.0357	20.0175	0.0042	0.0121	20.0052	0.005 86
AVG DIFF	0.0000	20.1648	20.0070	0.0023	20.0110	20.036 10

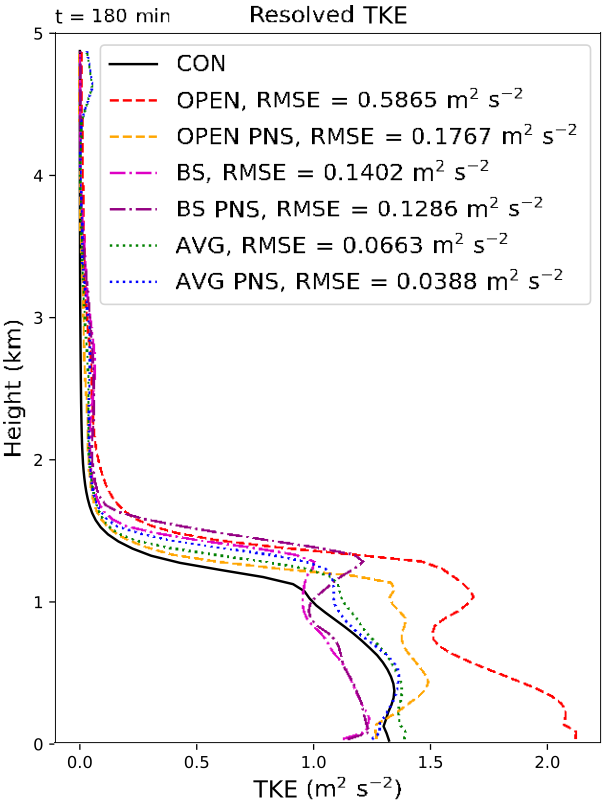

FIG. 14. As Fig. 10, but for the shear simulations.

across the entire horizontal extent of the domain (Fig. 15), due to the aforementioned cool bias for u and a positive bias for u (Figs. 15a,b). AVG continued to perform the best among simulations that did not use periodic north–south LBCs across the entire domain; however, unlike in the no-shear simulations, AVG with shear resulted in a slightly higher hh than AVG PNS for u in the western 70 km of the domain (Fig. 15b). Finally, the behavior of OPEN and OPEN PNS were similar to the simulations without shear where OPEN PNS generally improved hh for u, u, and y by using periodic north–south LBCs (Figs. 15a–c). That said, the most pronounced difference in rank between the shear and no-shear simulations was for the OPEN PNS simulations, which had the second lowest TKE RMSE with no shear and the second highest TKE RMSE with shear (Figs. 10, 14).

Temporal evolution of hh was also generally consistent between the shear and no-shear simulations (Fig. 16). However, three notable differences for the shear simulations relative to the no-shear simulations can be seen in hh for u (cf. Fig. 16b and Fig. 12b), including a period of higher hh for BS and BS PNS around t 5 20–80 min that is most pronounced from 30 to 40 min, a slight improvement for AVG after t 5 120 min, and a slight decrease in hh for AVG PNS after t 5 155 min. It is not surprising that the primary differences arise in u given the shear profile. Differences in hh between the shear and no-shear simulations are relatively minor for other variables.

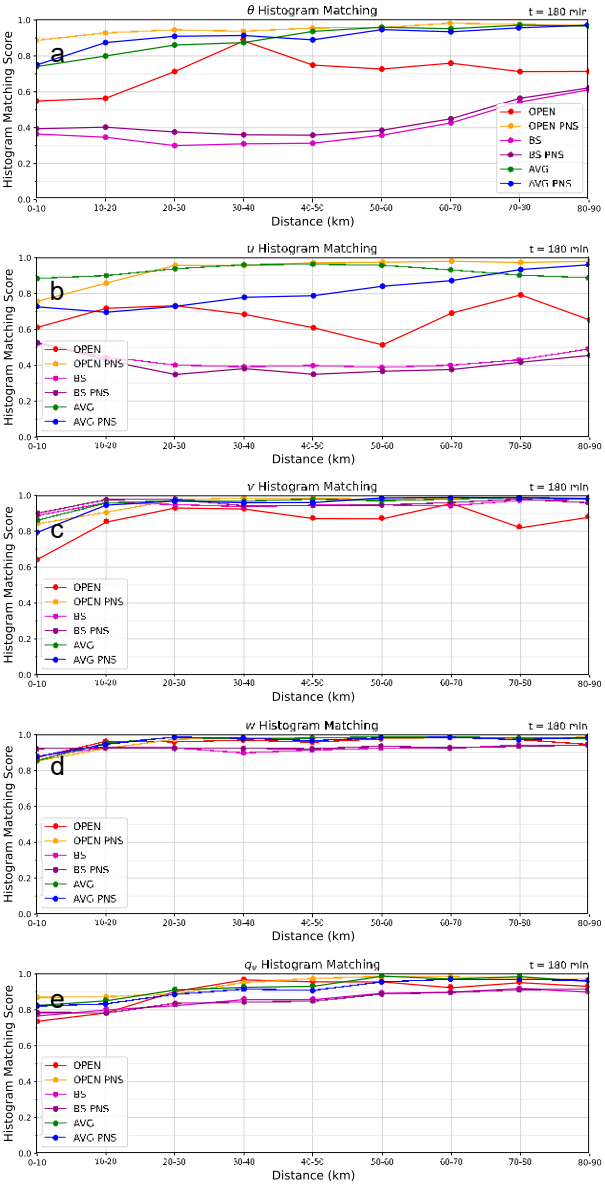

FIG. 15. As Fig. 11, but for the shear simulations.

4. Discussion

Caveats to consider are that these simulations were performed for daytime (1500 to 1800 UTC), midsummer (15 July), in the Great Plains (408, 21008), over a surface type of irrigated cropland and pasture, using a pseudo-two-dimensional domain (10 km south–north, 90.4 km west–east), and under a limited set of initial conditions, and so any changes to this configuration could result in differences in relative performance for each LBC option. Overall, the conditions described above favored a CBL consisting of open-cell convection (no-shear simulation) or horizontal convective rolls (shear simulation). Use of different initial conditions or model settings could result in different convective organization that may impact relative performance

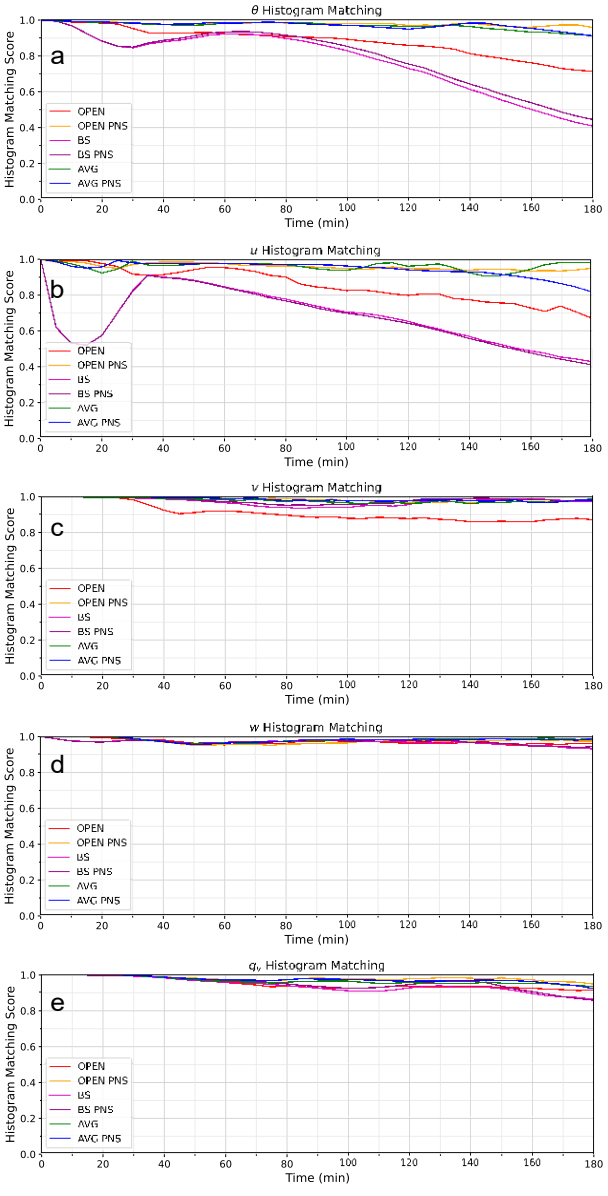

FIG. 16. As Fig. 12, but for the shear simulations.

of the nudging techniques. Specific implications are mentioned as appropriate in the following paragraphs.

In the absence of inflow nudging, or any other method described in the introduction, OPEN is the default for nonperiodic LBCs. As expected, the deficiencies in this method described in the introduction resulted in substantial error in CBL representation relative to CON in both no-shear and sheared simulations. Of all test simulations completed, OPEN was a clear outlier in terms of its poor representation of resolved TKE, with an RMSE 5 0.8616 and 0.5865 $m^2 s^{22}$ for the no-shear and shear simulations, respectively. In the case of the no-shear simulations, this RMSE is approximately 6.5 times as great as the RMSE for any of the other no-shear simulations completed for this study (Fig. 10). OPEN was also characterized by a low mean hh across all variables at 180 min and a decreasing hh for u, u, and y at the end of the simulation for no-shear (Table 3, Figs. 12a–c) and sheared simulations (Table 4, Figs. 16a–c).

Analyses showed that OPEN had relatively low matching scores near the upstream boundary, particularly for u, y, and q_y in the simulations without shear (Fig. 11); this deficiency could also be seen in the 25 m AGL plan views for theta and y (Figs. 4d, 6d). A key difference between the OPEN simulations with and without shear is that u had a lower hh in the western 10 km of the domain in the shear simulation, in addition to the low hh scores for u, y, and q_y (Fig. 15). The trend in hh with increased distance from the upstream lateral boundary is inconsistent for OPEN simulations, especially for u, theta, and, to a lesser extent, y. This suggests that, while improvements in convective structure with increased distance from the upstream boundary appear to be realistic in comparison with CON, the statistical nature of the convection does not actually compare well to CON. Using OPEN for simulations that explicitly represent turbulent structures in the boundary layer will result in errors in the representation of convective processes. These errors may have implications on the evolution of simulated mesoscale phenomena, and use of inflow nudging is advised.

Starting with CM1 release 19.8, an inflow-nudging method was available to nudge inflow toward the base-state wind profile. Of the simulations performed for the current study, the simulation that nudged inflow to the BS had the lowest mean hh score for both the no-shear (Table 3) and shear (Table 4) simulations. This makes sense when considering that any simulation with friction will consist of nonzero domainwide averaged tendencies in kinematic variables, with implications on the evolution of thermodynamic variables. A bias was seen in u due to the semislip bottom boundary condition, which acted to decrease its magnitude near the surface, and generally within the CBL due to mixing as the simulation progressed (Figs. 12b, 16b). This bias resulted in convergence, ascent, and cooling, particularly in western portions of the domain (Figs. 12a, 16a). As was the case for OPEN and OPEN shear, BS and BS shear also had a decreasing trend in hh for u and u toward the end of the simulation. Caveats worth noting are that the date, time, surface type, and wind profile will all influence the evolution relative to CON through their influence on radiative forcing, fluxes, resultant tendencies, and organization of convection. For example, smaller errors in u would be expected for BS at times with weaker radiative forcing, resulting from a decrease in the depth of the convective boundary layer. Errors in y were much smaller than u overall, since the base-state value for y was 0 m s^{21} at every vertical level in both the no-shear and shear simulations. We would expect lower histogram matching scores for y if larger magnitudes of y were included in the base-state wind profiles. Despite the overall poor histogram matching scores for BS, there was some improvement in the resolved TKE profile, with an RMSE 5 0.1118 $m^2 s^{22}$ for BS and an RMSE 5 0.1402 $m^2 s^{22}$ for BS shear, as opposed to 0.8616 $m^2 s^{22}$ for OPEN and 0.5865 $m^2 s^{22}$ for OPEN shear (Figs. 10, 14). In cases where a temporally consistent wind profile is needed, there are some benefits of

employing BS. However, improvements in kinematics through BS come at the cost of thermodynamic deficiencies.

The new technique implemented by the authors within CM1 (see section 2a) employed the same nudging principles used to nudge the upstream boundary to the base state, however, the prescribed inflow values were nudged to a continually updating horizontal average for each vertical level. The horizontal-average nudging technique allows inflow properties to evolve with the rest of the domain under the influence of radiation, surface fluxes, and friction, resulting in a more realistic representation of a CBL. This new method resulted in substantial improvements in AVG relative to OPEN and BS in both simulations with and without shear, as AVG had the highest mean hh across all variables (Tables 3 and 4) and the best representation of resolved TKE ($RMSE_{noshear} = 0.1061\ m^2\ s^{-2}$; $RMSE_{shear} = 0.0663\ m^2\ s^{-2}$) among the simulations with consistent LBCs on all lateral boundaries (Figs. 10, 14). Unlike OPEN, hh for AVG and AVG shear increased with increasing distance from the upstream lateral boundary for all variables (Figs. 11, 15), except for a slight decrease for u at the end of the shear simulation. Moreover, improvements in hh for AVG and AVG shear relative to OPEN and OPEN shear were particularly large in the upstream (western) 20 km of the domain. The improvements in hh near the upstream lateral boundary for AVG are consistent with the decreased inward extent of unrealistic laminar structures visible in Figs. 4–6. There was some decrease in hh for AVG later in the simulation, the decrease was much less pronounced than in OPEN or BS (Figs. 12, 16). Based on these clear improvements over OPEN and BS, use of nudging to a continually updating horizontal average is recommended for simulations of CBL, when use of periodic LBCs is not feasible.

For the simulations without shear, improvements in hh were seen when using periodic LBCs on the south and north lateral boundaries (i.e., OPEN PNS, BS PNS, and AVG PNS). AVG PNS had the highest mean hh among all six no-shear simulations, followed closely by OPEN PNS; the improvement in mean hh for BS PNS relative to BS was minor (hh = 0.0050; Table 3). In terms of resolved TKE, AVG PNS most closely matched CON (RMSE = 0.0627 $m^2\ s^{-2}$), followed by OPEN PNS (RMSE = 0.0808 $m^2\ s^{-2}$). Interestingly, RMSE increased to 0.1317 $m^2\ s^{-2}$ for BS PNS, relative to 0.1118 $m^2\ s^{-2}$ for BS. For the shear simulations, the TKE RMSE difference is more consistent with PNS simulations all having lower TKE RMSE relative to their non-PNS counterparts. While use of PNS LBCs improves hh and representation of resolved TKE for OPEN and AVG without shear, it is important to note that use of PNS LBCs should be limited to simulations of phenomena that are pseudo-two-dimensional in nature.

For domains consisting of multiple air masses (thunderstorm outflow, sea-breeze fronts, etc.) inflow nudging will need to be adjusted so that inflow is nudged to an average wind profile computed within its respective air mass. For example, a sea-breeze simulation on a pseudo-two-dimensional domain should compute two representative profiles}one over land and one over water. Both averages should be computed in areas where any turbulence is fully "spun up," and the land average should be far enough inland so that any sea-breeze front that develops does not enter the averaging area. This configuration of averaging areas would eliminate the possibility of characteristics from one air mass being used to nudge an inflow boundary that is located within a separate air mass. In addition, if simulating deep convection, the averaging area must not include areas where perturbations are included to induce convection initiation (e.g., warm bubble). An exhaustive list of situations and specific guidance for nudging is not provided here, as appropriate regions to compute average profiles will vary based on the domain size and phenomena under consideration.

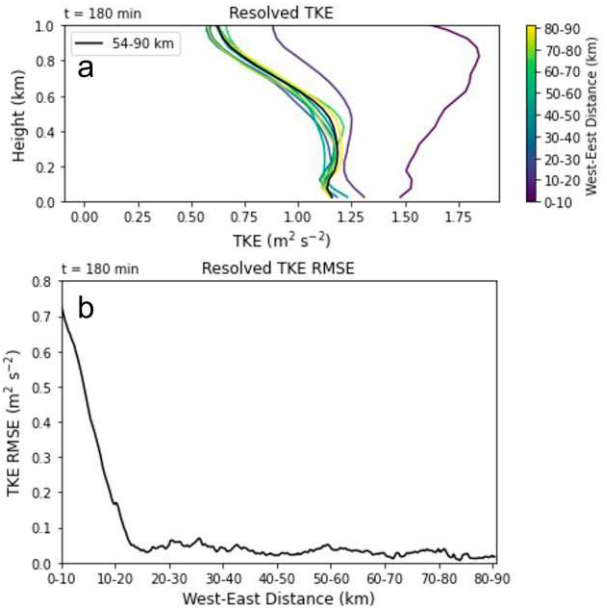

FIG. 17. (a) Resolved TKE in the lowest 975 m of the AVG simulation, with mean values computed for 10-km subsets of the domain (colors), and the corresponding mean profile computed between 54 km and the eastern lateral boundary (black). (b) TKE RMSE for the lowest 975 m relative to the black profile in (a), computed for 10-km subsets of the domain (0–10, 0.1–10.1 km, etc.).

The analyses provided here used dual-periodic control simulations to evaluate the relative performance of simulations using various open lateral boundary condition options. However, a single dual-periodic control simulation is not possible for model domains that consist of more than one air mass or surface type, and thus no independent simulation for comparison exists to determine what portion of the domain is fully "spun up" (i.e., computation of hh or TKE RMSE). That said, knowledge of the rate of inflow at the upstream lateral boundary can be used to determine what region of the domain has not been affected by laminar inflow, and thus can be used as a point for comparison for TKE RMSE or hh. In the interest of brevity, analysis of TKE is shown from the no-shear AVG simulation, where the base-state u and y were 5 and 0 m s^{-1}, respectively. Assuming a constant inflow at the upstream lateral boundary, the maximum inward extent of inflow for the 180-min simulation is 54 km (this is likely an overestimate, since the influence of friction decreased the near-surface u as

the simulation progressed). Based on these assumptions, the area between 54 km and the eastern boundary can be considered a control, as that portion of the domain is unaffected by the unrealistic laminar region at and near the western boundary. For example, Fig. 17a includes mean TKE profiles from this simulation computed for 10-km-wide subsets of the domain, starting at the upstream (west) boundary, and compares them with the mean TKE profile between 54 km and the downstream (eastern) boundary. Use of the 10-km-wide moving average ensured that the average profiles were representative of a portion of the domain, rather than being heavily impacted by individual thermals or other small-scale features. In Fig. 17b, RMSE values for increasing distance from the upstream lateral boundary are shown. In this example, TKE RMSE decreases rapidly until stabilizing at low RMSE values after approximately the 13–23-km interval, suggesting that the model is fully "spun up" by 13 km into the domain. While not shown here, in cases with stronger winds in the CBL, such as the shear simulations, we suggest the analysis be completed with both the mean CBL wind and the maximum CBL wind to determine the distance into the domain an air parcel at the inflow boundary will have traversed since model initialization. While the authors' analysis is shown for t 5 180 min, it may be reasonable to complete this analysis for any time after the model has spun up. This may be necessary for simulations with extremely strong winds in the CBL.

5. Summary

In recent years, the mesoscale modeling community has increased its use of idealized simulations that include realistic CBL turbulence, through inclusion of radiative forcing, surface fluxes, representation of friction (e.g., semislip surface), and small random perturbations to u at initialization to enable development of convection. Absent use of periodic LBCs, areas of inflow are laminar in nature and have been shown to exhibit unrealistic structures. Starting with release 19.8, CM1 includes an option to nudge inflow to the base-state wind profile in simulations with open LBCs. In this paper, we evaluated the potential use of this and other inflow-nudging options to improve the representation of CBL thermodynamics and kinematics in environments with and without vertical wind shear. Simulations with and without inflow nudging were run to evaluate their performance relative to respective shear or no-shear dual-periodic LBC control simulations. The domain for these simulations was pseudo-two-dimensional (90.4 km 3 10 km 3 5 km in the west–east, south–north, and vertical dimensions), lending itself to two sets of experiments for each vertical profile of wind. The first set of experiments employed consistent LBCs on all lateral boundaries, including OPEN, open with nudging to the BS, and AVG. The technique to nudge inflow toward the domain-averaged profile was introduced in this paper, based on the base-state nudging option in CM1. The second set of experiments used the same LBCs on the west and east lateral boundaries as the first set, with periodic LBCs used on the north and south boundaries (OPEN PNS, BS PNS, and AVG PNS). All simulations included radiative forcing, surface fluxes, and a semislip surface, and used a common thermodynamic profile. The vertical wind profile consisted of either no vertical wind shear ($u = 5\ m\ s^{-1}$; $v = 0\ m\ s^{-1}$) or $4\ m\ s^{-1}\ km^{-1}$ of vertical wind shear in u with $u_{sfc} = 5\ m\ s^{-1}$ and $v = 0\ m\ s^{-1}$. In the control simulations, use of periodic LBCs enabled development of open-cell convection (no shear control) or horizontal convective rolls (shear control) throughout the domain, whereas use of any type of open LBCs resulted in a region of laminar inflow that eventually transitions into open-cell convection or horizontal convective rolls. The distance from the upstream lateral boundary required for convection to fully spin up varied across the simulations, ranging from approximately 10–20 km downstream of the upstream boundary. The evolution of open LBC simulations with and without nudging were compared with their respective shear or no-shear dual-periodic control simulation using a histogram matching score and the domain-averaged profile of resolved TKE within the boundary layer. Analyses described in this paper support the following conclusions relating to the choice of LBCs:

- While unrealistic structures appear to be limited to areas near the upstream boundary, we have shown that use of open LBCs with no inflow nudging results in deficiencies in representation of resolved TKE and poor representation of thermodynamics and kinematics throughout the domain. Thus, use of open LBCs without inflow nudging is not recommended for simulations with realistic CBL structures.
- Histogram matching scores calculated for 10-km-wide subsets of the domain show that the inward extent of the laminar inflow region decreases when nudging inflow to either the base state or horizontal average profiles, with a more pronounced decrease in extent for average profile inflow nudging.
- While the extent of laminar inflow near the upstream lateral boundary is decreased through inflow-nudging, some laminar flow remains. Users of these methods should exclude the laminar inflow region from analyses.
- Use of inflow nudging to the base state serves its intended purpose of maintaining a more consistent wind profile. However, this can result in an area of low-level convergence near the upstream boundary with resultant ascent and an associated cool bias. In these experiments, this results in low histogram matching scores relative to the dual-periodic control simulation.
- The newly developed horizontal average inflow nudging technique on open LBCs performed most similar to the dual-periodic control simulation in terms of resolved TKE and mean histogram matching score, among simulations with consistent LBCs on all lateral boundaries. Use of this method is recommended for simulations of CBL phenomena that are not pseudo–two dimensional in nature.
- Mean histogram matching scores increased and inward extent of laminar inflow decreased when employing periodic boundary conditions on the south and north (cross stream) lateral boundaries in combination with open, open with inflow nudging to the base state, and open with inflow nudging to the horizontal average profile on west and east (upstream and

downstream) lateral boundaries. The lone exception to this result was between the mean histogram matching scores of AVG and AVG PNS with shear, as AVG with shear had a slightly higher mean histogram matching score than AVG PNS with shear. However, use of periodic LBCs may not be feasible depending on the phenomena being simulated.

- Overall, use of inflow nudging to the horizontal average profile on the upstream lateral boundary with periodic LBCs on the south and north lateral boundaries results in the lowest error in resolved TKE and either the highest (no shear) or second highest (shear) mean histogram matching scores. Thus, use of this method is recommended for simulations of CBL phenomena that are pseudo–two dimensional in nature.

In closing, use of inflow nudging to the horizontal average is recommended for simulations that include realistic CBL, while needing to use open lateral boundary conditions due to the domain consisting of either multiple air masses or surface types. Use of open lateral boundary conditions or open with inflow nudging to the base state result in errors in thermodynamic and kinematic properties when simulations include realistic CBL turbulent structures. Future work is needed to adapt the inflow-nudging technique for cases where conditions require different inflow-nudging profiles for individual lateral boundaries due to the presence of airmass boundaries within the domain.

Acknowledgments. This work has been supported by National Science Foundation Grant AGS-2113324. The authors thank Dr. George Bryan for providing and maintaining the CM1 source code and Dr. Daria Kluver of Central Michigan University for valuable discussion on the histogram matching score method. This work used the Extreme Science and Engineering Discovery Environment (XSEDE; Towns et al. 2014), which is supported by National Science Foundation Grant ACI-1548562. The numerical simulations were performed on Stampede 2 at the Texas Advanced Computing Center (TACC) at the University of Texas at Austin through XSEDE allocation TG-ATM190021. Author C. H. Boyer was supported by the Earth and Ecosystem Science doctoral program at Central Michigan University. The authors are grateful for the editor, an anonymous reviewer, and Dr. Matt Flournoy for their helpful feedback to improve the paper.

Data availability statement. CM1 source code is available from NCAR. The CM1 source code and namelists used for the simulations in this study are available upon request.

REFERENCES

Atkins, N. T., R. M. Wakimoto, and T. M. Weckwerth, 1995: Observations of the sea-breeze front during CaPE. Part II: Dual-doppler and aircraft analysis. Mon. Wea. Rev., 123, 944–969, https://doi.org/10.1175/1520-0493(1995)123,0944:OOTSBF.2.0.CO;2.

Bluestein, H. B., J. B. Houser, M. M. French, J. C. Snyder, G. D. Emmitt, I. Popstefanija, C. Baldi, and R. T. Bluth, 2014: Observations of the boundary layer near tornadoes and in supercells using a mobile, collocated, pulsed Doppler lidar and radar. J. Atmos. Oceanic Technol., 31, 302–325, https://doi.org/10.1175/JTECH-D-13-00112.1.

Bryan, G. H., and J. M. Fritsch, 2002: A benchmark simulation for moist nonhydrostatic numerical models. Mon. Wea. Rev., 130, 2917–2928, https://doi.org/10.1175/1520-0493(2002)130,2917:ABSFMN.2.0.CO;2.

} } , N. A. Dahl, D. S. Nolan, and R. Rotunno, 2017: An eddy injection method for large-eddy simulations of tornado-like vortices. Mon. Wea. Rev., 145, 1937–1961, https://doi.org/10.1175/MWR-D-16-0339.1.

Dailey, P. S., and R. G. Fovell, 1999: Numerical simulation of the interaction between the sea-breeze front and horizontal convective rolls. Part I: Offshore ambient flow. Mon. Wea. Rev., 127, 858–878, https://doi.org/10.1175/1520-0493(1999)127,0858:NSOTIB.2.0.CO;2.

Davenport, C. E., C. L. Ziegler, and M. I. Biggerstaff, 2019: Creating a more realistic idealized supercell thunderstorm evolution via incorporation of base-state environmental variability. Mon. Wea. Rev., 147, 4177–4198, https://doi.org/10.1175/MWR-D-18-0447.1.

Davies-Jones, R., 2021: Invented forces in supercell models. J. Atmos. Sci., 78, 2927–2939, https://doi.org/10.1175/JAS-D-21-0082.1.

Dawson, D. T., II., B. Roberts, and M. Xue, 2019: A method to control the environmental wind profile in idealized simulations of deep convection with surface friction. Mon. Wea. Rev., 147, 3935–3954, https://doi.org/10.1175/MWR-D-18-0462.1.

Fovell, R. G., 2005: Convective initiation ahead of the sea-breeze front. Mon. Wea. Rev., 133, 264–278, https://doi.org/10.1175/MWR-2852.1.

} } , and P. S. Dailey, 2001: Numerical simulation of the interaction between the sea-breeze front and horizontal convective rolls. Part II: Alongshore ambient flow. Mon. Wea. Rev., 129, 2057–2072, https://doi.org/10.1175/1520-0493(2001)129,2057:NSOTIB.2.0.CO;2.

Friedrich, K., D. E. Kingsmill, C. Flamant, H. V. Murphey, and R. M. Wakimoto, 2008a: Kinematic and moisture characteristics of a nonprecipitating cold front observed during IHOP. Part I: A cross-front structures. Mon. Wea. Rev., 136, 147–172, https://doi.org/10.1175/2007MWR1908.1.

} } , } } , } } , } } , and } } , 2008b: Kinematic and moisture characteristics of a nonprecipitating cold front observed during IHOP. Part II: Alongfront structures. Mon. Wea. Rev., 136, 3796–3821, https://doi.org/10.1175/2008MWR2360.1.

Gaudet, B., A. Deng, D. Stauffer, and N. Seaman, 2012: Eddy seeding for improved WRF-LES simulations using realistic lateral boundary conditions. 13th WRF User's Workshop, Boulder, CO, NCAR 3.5, https://www2.mmm.ucar.edu/wrf/users/workshops/WS2012/ppts/3.5.pdf.

Helfand, H. M., and E. Kalnay, 1983: A model to determine open or closed cellular convection. J. Atmos. Sci., 40, 631–650, https://doi.org/10.1175/1520-0469(1983)040,0631:AMTDOO.2.0.CO;2.

Keeler, J. M., B. F. Jewett, R. M. Rauber, G. M. McFarquhar, R. M. Rasmussen, L. Xue, C. Liu, and G. Thompson, 2016: Dynamics of cloud-top generating cells in winter cyclones. Part I: Idealized simulations in the context of field observations. J. Atmos. Sci., 73, 1507–1527, https://doi.org/10.1175/JAS-D-15-0126.1.

Kingsmill, D. E., 1995: Convection initiation associated with a sea-breeze front, a gust front, and their collision. Mon. Wea. Rev., 123, 2913–2933, https://doi.org/10.1175/1520-0493(1995)123,2913:CIAWAS.2.0.CO;2.

Koch, J., M. C. Demirel, and S. Stisen, 2018: The SPAtial EFficiency metric (SPAEF): Multiple-component evaluation of spatial patterns for optimization of hydrological models. Geosci. Model Dev., 11, 1873–1886, https://doi.org/10.5194/gmd-11-1873-2018.

Lund, T. S., X. Wu, and K. D. Squires, 1998: Generation of turbulent inflow data for spatially-developing boundary layer simulations. J. Comput. Phys., 140, 233–258, https://doi.org/10.1006/jcph.1998.5882.

Lyza, A. W., and K. R. Knupp, 2018: A background investigation of tornado activity across the Southern Cumberland Plateau Terrain System of Northeastern Alabama. Mon. Wea. Rev., 146, 4261–4278, https://doi.org/10.1175/MWR-D-18-0300.1.

Markowski, P. M., N. T. Lis, D. D. Turner, T. R. Lee, and M. S. Buban, 2019: Observations of near-surface vertical wind profiles and vertical momentum fluxes from VORTEX-SE 2017: Comparisons to Monin–Obukhov similarity theory. Mon. Wea. Rev., 147, 3811–3824, https://doi.org/10.1175/MWR-D-19-0091.1.

Mayor, S. D., P. R. Spalart, and G. J. Tripoli, 2002: Application of a perturbation recycling method in the large-eddy simulation of a mesoscale convective internal boundary layer. J. Atmos. Sci., 59, 2385–2395, https://doi.org/10.1175/1520-0469(2002)059,2385:AOAPRM.2.0.CO;2.

Mirocha, J., B. Kosović, and G. Kirkil, 2014: Resolved turbulence characteristics in large-eddy simulations nested within mesoscale simulations using the Weather Research And Forecasting model. Mon. Wea. Rev., 142, 806–831, https://doi.org/10.1175/MWR-D-13-00064.1.

Miura, Y., 1986: Aspect ratios of longitudinal rolls and convection cells observed during cold air outbreaks. J. Atmos. Sci., 43, 26–39, https://doi.org/10.1175/1520-0469(1986)043,0026:AROLRA.2.0.CO;2.

Muñoz-Esparza, D., B. Kosović, J. Mirocha, and J. van Beeck, 2014: Bridging the transition from mesoscale to microscale turbulence in numerical weather prediction models. Bound.-Layer Meteor., 153, 409–440, https://doi.org/10.1007/s10546-014-9956-9.

Nowotarski, C. J., P. M. Markowski, Y. P. Richardson, and G. H. Bryan, 2014: Properties of a simulated convective boundary layer in an idealized supercell thunderstorm environment. Mon. Wea. Rev., 142, 3955–3976, https://doi.org/10.1175/MWR-D-13-00349.1.

} } , } } , } } , and } } , 2015: Supercell low-level mesocyclones in simulations with a sheared convective boundary layer. Mon. Wea. Rev., 143, 272–297, https://doi.org/10.1175/MWR-D-14-00151.1.

Peckham, S. E., R. B. Wilhelmson, L. J. Wicker, and C. L. Ziegler, 2004: Numerical simulation of the interaction between the dryline and horizontal convective rolls. Mon. Wea. Rev., 132, 1792–1812, https://doi.org/10.1175/1520-0493(2004)132,1792:NSOTIB.2.0.CO;2.

Sever, G., R. Kotamarthi, and Y. Feng, 2019: A turbulence library for asynchronous coupling of meso- and microscale models. 10th Conf. on Weather, Climate, and the New Energy Economy, Phoenix, AZ, Amer. Meteor. Soc, 2.3. https://ams.confex.com/ams/2019Annual/meetingapp.cgi/Paper/353328.

Skyllingstad, E. D., D. Vickers, L. Mahrt, and R. Samelson, 2007: Effects of mesoscale sea-surface temperature fronts on the marine atmospheric boundary layer. Bound.-Layer Meteor., 123, 219–237, https://doi.org/10.1007/s10546-006-9127-8.

Spalart, P. R., and A. Leonard, 1985: Direct numerical simulation of equilibrium turbulent boundary layers. Proc. Fifth Symp. on Turbulent Shear Flows, Ithaca, NY, Cornell University, 9.35–9.40, https://ui.adsabs.harvard.edu/abs/1985stsf.procR...9S/abstract.

Swain, M. J., and D. H. Ballard, 1991: Color indexing. Int. J. Comput. Vision, 7, 11–32, https://doi.org/10.1007/BF00130487.

Towns, J., and Coauthors, 2014: XSEDE: Accelerating scientific discovery. Comput. Sci. Discovery, 16, 62–74, https://doi.org/10.1109/MCSE.2014.80.

Xue, M., and W. J. Martin, 2006a: A high-resolution modeling study of the 24 May 2002 dryline case during IHOP. Part I: Numerical simulation and general evolution of the dryline and convection. Mon. Wea. Rev., 134, 149–171, https://doi.org/10.1175/MWR3071.1.

} } , and } } , 2006b: A high-resolution modeling study of the 24 May 2002 dryline case during IHOP. Part II: Horizontal convective rolls and convective initiation. Mon. Wea. Rev., 134, 172–191, https://doi.org/10.1175/MWR3072.1.